Available online at www.sciencedirect.com
ScienceDirect
Trans. Nonferrous Met. Soc. China 23(2013) 2422−2430
Transactions of Nonferrous Metals Society of China
www.tnmsc.cn

Synthesis of nickel ferrite precursors from low grade nickel matte

Li-hua HE[1], Zhong-wei ZHAO[1], You-xin ZHANG[1,2]

1. School of Metallurgy and Environment, Central South University, Changsha 410083, China;
2. Jinchun Group Co., Ltd., Jinchang 737104, China

Received 23 July 2012; accepted 8 May 2013

Abstract: Fine nickel ferrite precursors $NiFe_2(C_2O_4)_3·6H_2O$ were obtained via co-precipitation method with low grade nickel matte as the raw material. Thermodynamic analysis of $NiCl_2$−$FeCl_2$−$(NH_4)_2C_2O_4$−H_2O system for precipitation identified that the theoretical optimum co-precipitation pH value is 2, and $C_2O_4^{2-}$ has strong complexation with Ni^{2+} and Fe^{2+} ions. Based on these theoretical considerations, the effects of parameters on the precipitation rates and precursors size were investigated systematically. The results show that the optimum co-precipitation conditions are pH=2, temperature 45 °C, 1.2 times theoretical amount of $(NH_4)_2C_2O_4$ dosage and 3% PEG400 addition. Under these conditions, the precipitation rates of Ni^{2+} and Fe^{2+} are both over 99.8%, with the precursors size of 1−2 um. Furthermore, X-ray diffraction (XRD) and thermogravimetry-differential thermal analysis (TG-DTA) demonstrate that the precursors are single-phase solid solution, wherein the nickel/iron atoms are replaced by the iron/nickel atoms reciprocally.

Key words: nickel ferrite; ferrite; magnetic materials; co-precipitation; low grade nickel matte

1 Introduction

Spinel nickel ferrite ($NiFe_2O_4$) is one of the most promising magnetic materials. It has been widely used in the aspects of magnetic recording media and magnetic fluids for the storage and/or retrieval of information, magnetic resonance imaging enhancement, catalysis, magnetically guided drug delivery, sensors and pigments due to its magnetic and electrical properties with chemical and thermal stabilities [1−3]. Conventionally, $NiFe_2O_4$ powders are prepared by solid-state reaction method at high temperatures with a repeated grinding [4−6]. However, this approach has some conspicuous disadvantages such as larger particle size, broader particle size distribution and impurities. In contrast, wet chemical preparation routes such as co-precipitation[7,8], sol−gel [9−11], hydrothermal[12,13] and microemulsion method [14,15], have an indisputable advantage over solid-state reactions in achieving better homogeneity, in which the starting compounds were mixed on molecular level. Especially the co-precipitation method, as a commercially feasible process, has attracted much attention recently.

Remarkably, in the traditional processes, the preparation of $NiFe_2O_4$ always uses high-purity metal salts as the raw materials, and it undoubtedly increases production costs. Therefore, finding a simple and cost-effective route to prepare $NiFe_2O_4$ is quite attractive. In recent years, some research works have focused on the direct synthesis technologies by using the smelting slag or metallic ores as the raw materials [16,17]. For instance, AHMED [18] synthesized a manganese ferrite from non-standard raw materials using ceramic technique. Coincidentally, RASHAD [19] also prepared a manganese ferrite by using low-grade manganese ore. Compared with the traditional processes, these direct methods have many significant advantages such as low cost, high resource utilization and friendly environment. And for the preparation of nickel ferrite $NiFe_2O_4$, it just needs Ni and Fe two resources. Fortunately, low-grade nickel matte, as an intermediate product of nickel smelting processes, mainly contains three elements, i.e. Ni, Fe and S [20,21]. If Ni and Fe in the nickel matte are dissolved into solution, then it is possible to synthesize $NiFe_2O_4$ via precipitation method.

So, the aim of the present work is the synthesis of $NiFe_2O_4$ precursors from low-grade nickel matte via

Foundation item: Project (2012BAB10B04) supported by National Key Technology R&D Program of China; Project supported by Hunan Provincial Innovation Foundation for Postgraduate, China
Corresponding author: Zhong-wei ZHAO; Tel: +86-731-88830476; E-mail: zhaozw@csu.edu.cn
DOI: 10.1016/S1003-6326(13)62750-8

co-precipitation method. The study focused on the effects of process parameters such as pH of the solution, reaction temperature, the addition of ammonium oxalate and surfactant on the synthesis of $NiFe_2O_4$ precursors. Moreover, the morphology and crystal structure of the produced powders were also examined.

2 Experimental

The precursors of spinel nickel ferrite were prepared by the oxalate coprecipitation method after leaching low grade nickel matte with $FeCl_3$ agent. Low grade nickel matte samples were provided by Jinchuan Group Co., Ltd., China, and its total chemical composition is listed in Table 1. Firstly, nickel matte sample was ground to <106 μm, and dissolved under the conditions of reaction temperature of 85 °C, reaction time of 2 h, $FeCl_3$ dosage of 1.2 times to theoretical value and HCl initial concentration of 1 mol/L, corresponding with the Ni extraction rate of 97.5%. Secondly, pyrite was added to the leaching solution to convert the excess Fe^{3+} into Fe^{2+}. During this process, the impurities such as Cu^{2+} and Pb^{2+} were removed simultaneously. Thirdly, after filtering the solution, and nickel chloride was added to the obtained filtrate for correction the Fe:Ni molar ratio to 2:1, and the chemical composition of the final solution is listed in Table 2. Finally, co-precipitation processes were operated under different pH values, reaction temperatures and polyethyleneglycol 400 (PEG 400) addition by using ammonium oxalate as the precipitant. Then the precipitated solution was filtered, washed several times with deionized water, and dried in a vacuum oven at 80 °C for 10 h.

Table 1 Chemical composition of low-grade nickel matte (mass fraction, %)

Ni	Fe	S
15.14	54.85	28.64

Table 2 Chemical composition of final solution ($g \cdot L^{-1}$)

Ni	Fe	Cu	Mg	Mn
26.78	51.00	0.002	0.004	0.008
Pb	Zn	Cr	Co	
0.004	0.009	0.012	0.005	

The chemical compositions of the raw materials and solutions were carried out via atomic absorption spectroscopy (WFX−120, Thermo Electron Corporation), the particle morphology was observed by SEM (JXA−8800R, JEOL Ltd.), the crystal structures of the samples were characterized by X-ray diffraction (XRD) with Cu K_α radiation (TTR III, Rigaku Corporation) at a speed of 4 (°)/min, and the TG−DTA curves of the samples were determined by SDTQ600 (TA Instrument Corporation) at a heating rate of 10 °C/min in air atmosphere with the flow rate of 100 mL/min.

3 Thermodynamic analysis

To get early insights into the properties and behaviors of the solution and find optimal conditions for precipitation, thermodynamic analysis of the $NiCl_2$−$FeCl_2$−$(NH_4)_2C_2O_4$−H_2O system was studied firstly. In this system, 34 ionic species were assumed to exist in the solution: H^+, OH^-, Cl^-, HCl, $C_2O_4^{2-}$, $HC_2O_4^-$, $H_2C_2O_4$(aq), NH_3, NH_4^+, Ni^{2+}, $Ni(OH)^+$, $Ni(OH)_2$(aq), $Ni(OH)_3^-$, NiC_2O_4(aq), $Ni(C_2O_4)_2^{2-}$, $Ni(C_2O_4)_3^{4-}$, $Ni(NH_3)^{2+}$, $Ni(NH_3)_2^{2+}$, $Ni(NH_3)_3^{2+}$, $Ni(NH_3)_4^{2+}$, $Ni(NH_3)_5^{2+}$, $Ni(NH_3)_6^{2+}$, $NiCl^+$, Fe^{2+}, $Fe(OH)^+$, $Fe(OH)_2$(aq), $Fe(OH)_3^-$, $Fe(OH)_4^{2-}$, FeC_2O_4(aq), $Fe(C_2O_4)_2^{2-}$, $Fe(C_2O_4)_3^{4-}$, $Fe(NH_3)^{2+}$, $Fe(NH_3)_2^{2+}$, $FeCl^+$, and 4 species as insoluble compounds were assumed to exist: NiC_2O_4(s), $Ni(OH)_2$(s), FeC_2O_4(s), $Fe(OH)_2$(s). This inventory leads to 37 equilibriums listed in Tables 3 and 4, in which equilibrium constant values were taken from Ref. [22].

For each equilibrium state, the concentration of each ion existing in the solution should not only satisfy its equilibrium reactions, but also the mass balance equations. In this work, the calculation model based on the Newton–Raphson iteration theory was carried out by using Microsoft Excel.

Generally, the oxalate dosage and solution pH value may play significant roles in the process of oxalate co-precipitation. Figure 1 shows the effect of oxalate concentration on Ni^{2+} and Fe^{2+} co-precipitation. It can be seen that the concentration of nickel decreases in the pH range of 0−1.5, yet increases from pH 1.5−5, and stays flat at pH 5−8 under a certain oxalate concentration. The theoretical optimum pH value is 1−2, corresponding with the $[Ni]_T$ value of 10^{-4} mol/L. In addition, it is worthy to note that if the pH value is lower than the theoretical optimum value, the higher oxalate concentration in solution, the lower total nickel concentration will be, and the opposite situation happens when the operated pH value is larger than the theoretical optimum. The tendency of Fe^{2+} in $\lg[Fe]_T$ vs pH (Fig. 1(b)) is similar to that of Ni^{2+} in $\lg[Ni]_T$ vs pH (Fig. 1(a)), and the theoretical optimum pH for Fe^{2+} precipitation is 2−3 with the $[Fe]_T$ value of $10^{-3.5}$mol/L.

These results can be explained by the effect of complexation, i.e. the oxalate existing mainly in the form of $H_2C_2O_4$ and/or $HC_2O_4^-$ in strong acid aqueous medium and $C_2O_4^{2-}$ in weak acid and alkaline solution. So, for the pH<2, higher oxalate concentration in the

Table 3 Equilibrium reactions for precipitation system at 25 °C

No.	Equilibrium reaction	lg *K*	No.	Equilibrium reaction	lg *K*
1	$Ni^{2+}+C_2O_4^{2-}=NiC_2O_4(s)$	9.4	17	$Fe^{2+}+C_2O_4^{2-}=FeC_2O_4(s)$	6.50
2	$Ni^{2+}+2OH^-=Ni(OH)_2(s)$	15.26	18	$Fe^{2+}+2OH^-=Fe(OH)_2(s)$	16.31
3	$Ni^{2+}+OH^-=Ni(OH)^+$	4.97	19	$Fe^{2+}+OH^-=Fe(OH)^+$	5.56
4	$Ni^{2+}+2OH^-=Ni(OH)_2(aq)$	8.55	20	$Fe^{2+}+2OH^-=Fe(OH)_2(aq)$	9.77
5	$Ni^{2+}+3OH^-=Ni(OH)_3^-$	11.33	21	$Fe^{2+}+3OH^-=Fe(OH)_3^-$	9.67
6	$Ni^{2+}+C_2O_4^{2-}=NiC_2O_4(aq)$	5.3	22	$Fe^{2+}+4OH^-=Fe(OH)_4^{2-}$	8.58
7	$Ni^{2+}+2C_2O_4^{2-}=Ni(C_2O_4)_2^{2-}$	7.64	23	$Fe^{2+}+C_2O_4^{2-}=FeC_2O_4(aq)$	2.9
8	$Ni^{2+}+3C_2O_4^{2-}=Ni(C_2O_4)_3^{4-}$	8.5	24	$Fe^{2+}+2C_2O_4^{2-}=Fe(C_2O_4)_2^{2-}$	4.52
9	$Ni^{2+}+NH_3=Ni(NH_3)^{2+}$	2.8	25	$Fe^{2+}+3C_2O_4^{2-}=Fe(C_2O_4)_3^{4-}$	5.22
10	$Ni^{2+}+2NH_3=Ni(NH_3)_2^{2+}$	5.04	26	$Fe^{2+}+NH_3=Fe(NH_3)^{2+}$	1.4
11	$Ni^{2+}+3NH_3=Ni(NH_3)_3^{2+}$	6.77	27	$Fe^{2+}+2NH_3=Fe(NH_3)_2^{2+}$	2.2
12	$Ni^{2+}+4NH_3=Ni(NH_3)_4^{2+}$	7.96	28	$Fe^{2+}+Cl^-=FeCl^+$	4.27
13	$Ni^{2+}+5NH_3=Ni(NH_3)_5^{2+}$	8.71	29	$H_2C_2O_4(aq)=H^++HC_2O_4^-$	−1.2727
14	$Ni^{2+}+6NH_3=Ni(NH_3)_6^{2+}$	8.74	30	$HC_2O_4^-=H^++C_2O_4^{2-}$	−4.27
15	$Ni^{2+}+Cl^-=NiCl^+$	−0.17	31	$NH_3+H^+=NH_4^+$	9.24
16	$HCl=H^++Cl^-$	6.2	32	$H_2O=H^++OH^-$	−14

Table 4 Mass balance equations for precipitation system at 25 °C

No.	Mass balance equation
1	$[Ni]_T=[Ni^{2+}]+[Ni(OH)^+]+[Ni(OH)_2(aq)]+[Ni(OH)_3^-]+[Ni(NH_3)^{2+}]+[Ni(NH_3)_2^{2+}]+[Ni(NH_3)_3^{2+}]+[Ni(NH_3)_4^{2+}]+[Ni(NH_3)_5^{2+}]+[Ni(NH_3)_6^{2+}]+[NiCl^+]+[NiC_2O_4(aq)]+[Ni(C_2O_4)_2^{2-}]+[Ni(C_2O_4)_3^{4-}]$
2	$[Fe]_T=[Fe^{2+}]+[Fe(OH)^+]+[Fe(OH)_2(aq)]+[Fe(OH)_3^-]+[Fe(OH)_4^{2-}]+[Fe(NH_3)^{2+}]+[Fe(NH_3)_2^{2+}]+[FeC_2O_4(aq)]+[Fe(C_2O_4)_2^{2-}]+[Fe(C_2O_4)_3^{4-}]+[FeCl^+]$
3	$[C]_T=[C_2O_4^{2-}]+[HC_2O_4^-]+[H_2C_2O_4(aq)]+[NiC_2O_4(aq)]+2[Ni(C_2O_4)_2^{2-}]+3[Ni(C_2O_4)_3^{4-}]+[FeC_2O_4(aq)]+2[Fe(C_2O_4)_2^{2-}]+3[Fe(C_2O_4)_3^{4-}]$
4	$[N]_T=[NH_3]+[NH_4^+]+[Ni(NH_3)^{2+}]+2[Ni(NH_3)_2^{2+}]+3[Ni(NH_3)_2^{2+}]+4[Ni(NH_3)_4^{2+}]+5[Ni(NH_3)_5^{2+}]+6[Ni(NH_3)_6^{2+}]+[Fe(NH_3)^{2+}]+2[Fe(NH_3)_2^{2+}]$
5	$[Cl]_T=[Cl^-]+[HCl]+[FeCl^+]+[NiCl^+]$

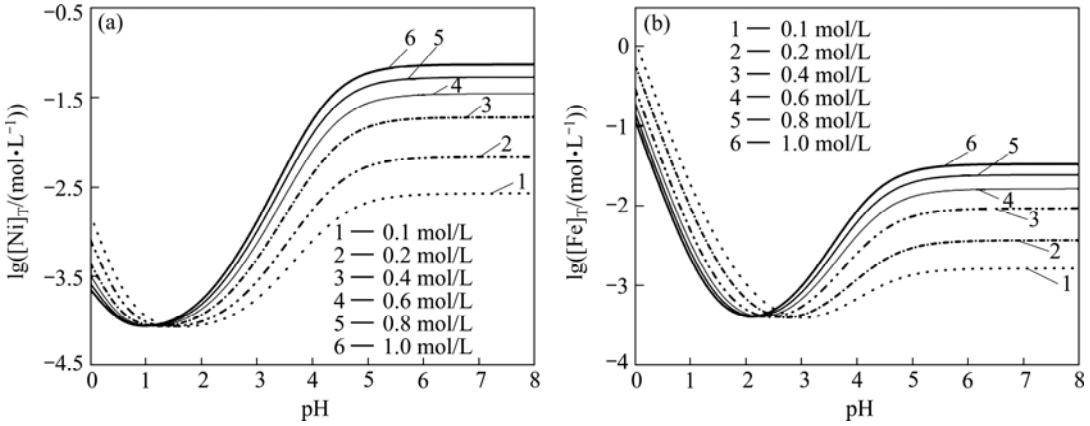

Fig. 1 Effect of oxalate concentrations on Ni^{2+} (a) and Fe^{2+} (b) precipitation

solution can provide more $C_2O_4^-$ ions, which is beneficial for Ni^{2+} and Fe^{2+} co-precipitation. But in alkaline solution, excess $C_2O_4^-$ will strongly coordinate with Ni^{2+} and Fe^{2+}, causing the obtained precipitate redissolution, which in turn leads to higher concentrations of $[Ni]_T$ and $[Fe]_T$ in solution. Actually, the coordination effect between Ni^{2+} and Fe^{2+} with $C_2O_4^{2-}$ can clearly be seen from Fig. 2. For Ni^{2+}, when

pH value ranges from 0 to 8, nickel in solution mainly exists in the forms of Ni^{2+}, $NiC_2O_4(aq)$, $Ni(C_2O_4)_2^{2-}$ and $Ni(C_2O_4)_3^{4-}$, and these for iron are Fe^{2+}, $FeC_2O_4(aq)$, $Fe(C_2O_4)_2^{2-}$ and $Fe(C_2O_4)_3^{4-}$ in order.

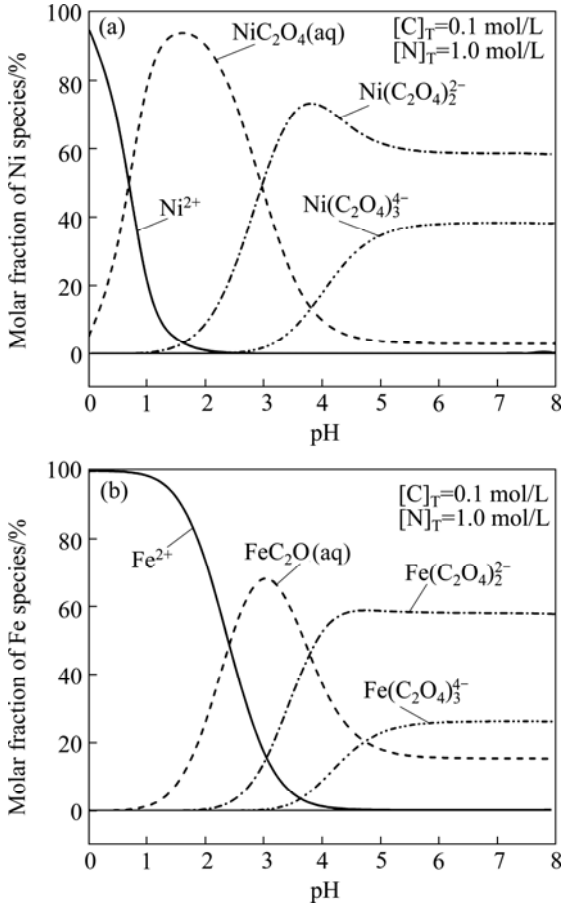

Fig. 2 Distribution of species containing Ni^{2+} (a) and Fe^{2+} (b) ions

Theoretically, in order to have a high Ni^{2+} and Fe^{2+} co-precipitation rate, it is essential to control the pH value precisely during the experiment.

4 Co-precipitation aspects

4.1 Effect of pH value

Based on the results of thermodynamic analysis, it is seen that the pH value has a major impact on the process of precipitation. Here, the precipitation experiments were carried out at pH 1, 1.5, 2, 2.5 and 3, respectively, with the reaction temperature of 55 °C, 1.2 times theoretical amount of $(NH_4)_2C_2O_4$ and aging time of 30 min. The effect of pH value on the Ni^{2+} and Fe^{2+} precipitation rate is shown in Fig. 3.

It can be seen that the precipitation rate of Ni is kept around 100%, and that of Fe gradually increases from 94.1% to 99.5% in the pH range of 1−2, while both decrease with the pH value increasing from 2 to 3. It is because that the concentration of free oxalate in these experiments is about 0.2 mol/L, and the theoretical total concentrations of Ni and Fe are 10^{-4} and $10^{-1.75}$−10^{-3} mol/L under the condition of pH 1−2 (Fig. 1), respectively. It is hard for the Fe^{2+} ions to precipitate completely, especially at lower pH value. When the pH value is higher than 2, the complexation between Ni^{2+}/Fe^{2+} and $C_2O_4^{2-}$ is strong, which causes higher nickel and iron concentration in solution, resulting in a lower precipitation rate.

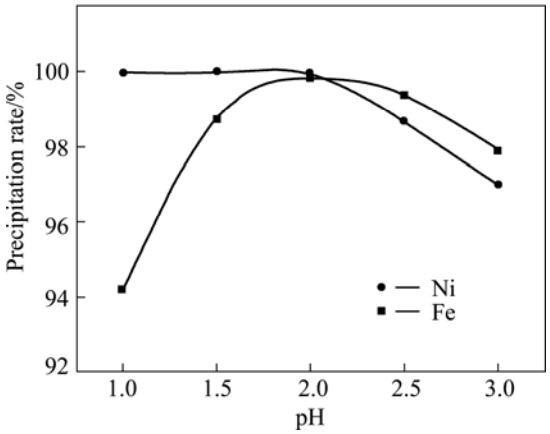

Fig. 3 Effect of pH on precipitation rates of Ni^{2+} and Fe^{2+}

Obviously, these experimental results are consistent with the information in the thermodynamic analysis. On the other hand, it also verifies the correctness of the theoretical analysis. In order to obtain $NiFe_2O_4$ powders in stoichiometric proportion, the optimum pH value is chosen to be 2.0. Under this condition, the precipitation rates of Ni^{2+} and Fe^{2+} are close.

4.2 Effect of $(NH_4)_2C_2O_4$ dosage

Figure 4 shows the influence of the amount of ammonium oxalate addition on the precipitation rates of Ni^{2+} and Fe^{2+} under the condition of 55 °C, pH value of 2.0 and aging time of 30 min. As observed from Fig. 4, with the increasing ammonium oxalate dosage, the

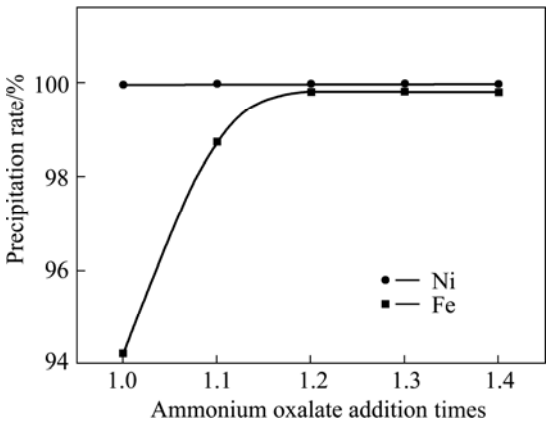

Fig. 4 Effect of ammonium oxalate addition on precipitation rates of Ni^{2+} and Fe^{2+}

precipitation rate of Ni^{2+} keeps constant (about 100%), and that of Fe^{2+} improves from 94.2% to 99.8%, and then gradually stabilizes at 99.8% when the quantity of $(NH_4)_2C_2O_4$ is over 1.2 times the theoretical value. This can be attributed to the difference of solubility product constant. More specifically, the solubility product constant of $NiC_2O_4(s)$ ($K_{sp}=10^{-9.4}$) is smaller than that of $FeC_2O_4(s)$ ($K_{sp}=10^{-6.5}$), as listed in Table 1, and the Ni^{2+} ion will be preferentially precipitated when the $(NH_4)_2C_2O_4$ precipitant is added into the solution. Therefore, in order to ensure the Ni^{2+} and Fe^{2+} ions homogeneous precipitation, the ammonium oxalate addition must be controlled to a certain range.

Furthermore, not only the precipitation rate, but also the particle size of the precursors can be influenced by the ammonium oxalate addition. The more ammonium oxalate is added, the smaller size of the precursors will be (Fig. 5). This can be attributed to the complexation of the excess $C_2O_4^{2-}$ with Ni^{2+} and Fe^{2+} in solution. On one hand, the complexation can avoid the grain growth too fast; On the other hand, it is helpful to refine the grain size and alleviate the particle agglomeration.

Taking both the precipitation rates and particle size into consideration, the dosage of $(NH_4)_2C_2O_4$ is chosen to be 1.2−1.3 times the theoretical value in this work.

4.3 Effect of precipitation temperature

Unlike pH value and ammonium oxalate addition, the temperature in the process of co-precipitation has no obvious effect on the precipitation rates of Ni^{2+} and Fe^{2+}, both of which are about 99.8% in the experimental temperature range of 35−75 °C, as listed in Table 5. Nevertheless, the particle size and distribution of the precursors are strongly influenced by the reaction temperature. According to the results presented in Fig. 6, fine and well-crystallized precursors powders are obtained at a lower temperature, and the size of precursors increases obviously with the rising temperature, accompanying with serious aggregation phenomenon. In this study, the optimum reaction temperature can be chosen as 20−45 °C.

4.4 Effect of PEG400 addition

As well as temperature, the effect of surfactant PEG 400 addition on the precipitate rates of Ni^{2+} and Fe^{2+} is puny (Table 6), and these results are similar with those of other research. In this work, both the precipitate rates of Ni^{2+} and Fe^{2+} are over 99.8%.

In fact, the main purpose of surfactant addition is to modify the size and distribution of the particles in the process of precipitation [23,24], rather than to improve the precipitation rate. As is well known, appropriate amount of surfactant addition is beneficial for obtaining smaller particles. As shown in Fig. 7, the precursors are severely agglomerated without PEG400, and the average particle size of precursors decreases with increasing PEG400 dosage. In this study, when the PEG400 dosage is 1% (mass fraction), the particle size is about 5 μm; as the PEG400 addition increases to 4%, the particle size is decreased to 1−2 μm.

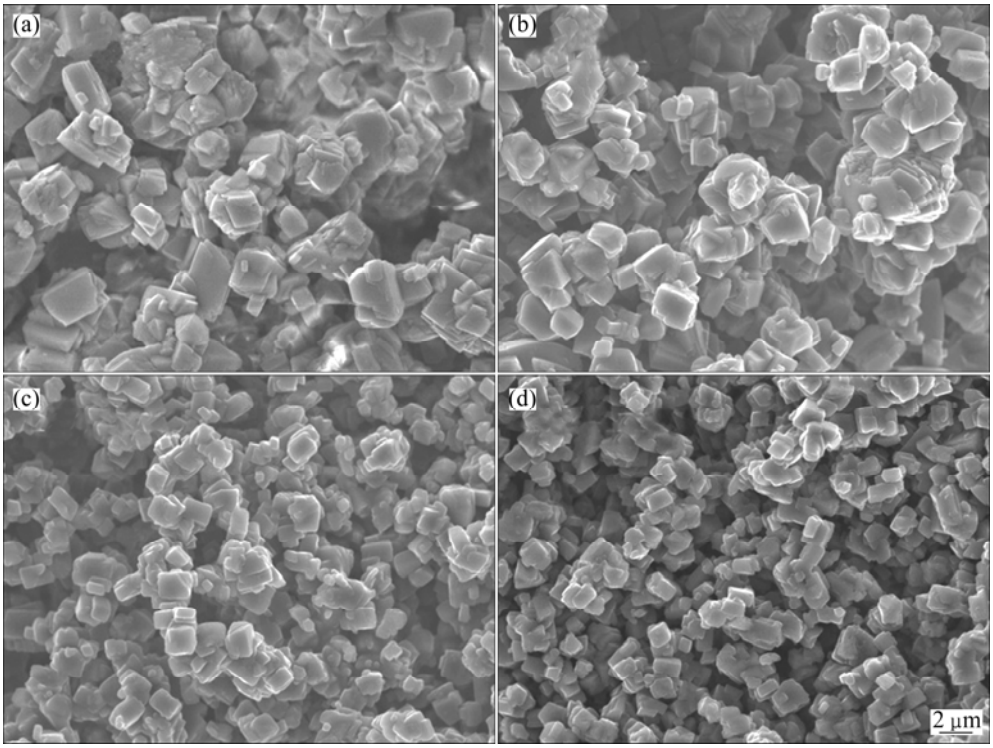

Fig. 5 SEM images of precursors obtained at different ammonium oxalate addition: (a) 1.0 times; (b) 1.1 times; (c) 1.3 times; (d) 1.4 times

Table 5 Effect of reaction temperature on precipitation rates of Ni^{2+} and Fe^{2+}

Temperature/ °C	Fe^{2+} precipitation rate/%	Ni^{2+} precipitation rate/%
35	99.82	99.92
45	99.88	99.92
55	99.84	99.97
65	99.89	99.96
75	99.92	99.94

Table 6 Effect of PEG400 addition on precipitation rates of Ni^{2+} and Fe^{2+}

PEG 400 addition/%	Fe^{2+} precipitation rate/%	Ni^{2+} precipitation rate/%
0	99.87	99.97
0.25	99.87	99.95
1	99.88	99.96
2	99.91	99.95
4	99.91	99.95

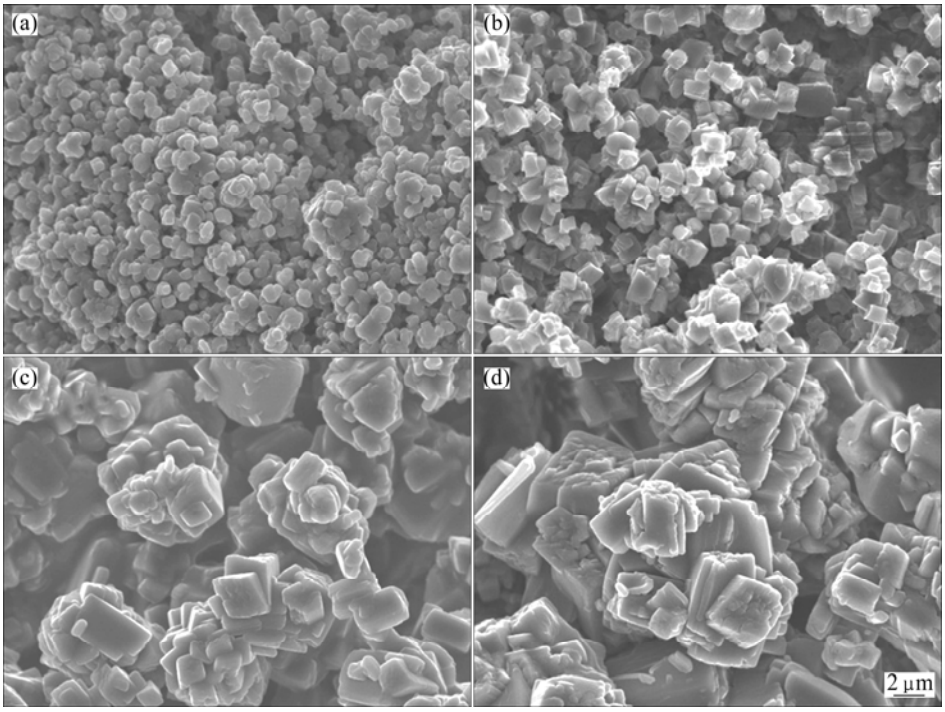

Fig. 6 SEM images of precursors obtained at different temperatures: (a) 35 °C; (b) 45 °C; (c) 65 °C; (d) 75 °C

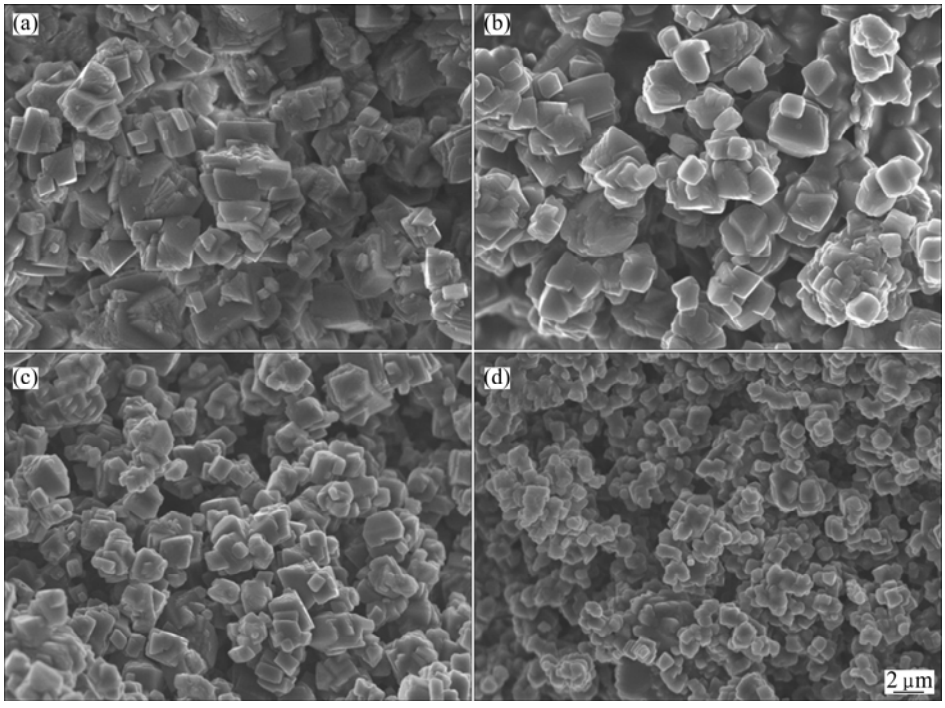

Fig. 7 SEM images of precursors obtained with different PEG400 addition: (a) 0; (b) 1%; (c) 2%; (d) 4%

4.5 Identification of Fe−Ni oxalate precursors

Generally, the properties of the $NiFe_2O_4$ product mainly depend on the morphology, purity and mixing degree of the precursors. Figure 10 shows the XRD patterns of the precursors obtained under the conditions of pH value of 2, temperature of 45 °C, $(NH_4)_2C_2O_4$ dosage 1.2 times of stoichiometric value, and 3% PEG400 addition. Figure 8 shows the X-ray diffraction pattern of the prepared precursors. It can be seen that the XRD peaks of the precursors are sharp, which means that the precursors are well-crystallized. However, these peaks do not match those of $NiC_2O_4·2H_2O$ (JCPDS#25−0581) or $FeC_2O_4·2H_2O$ (JCPDS#22−0355) exactly. By further studying the structure of the precursors, it is observed that the lattice parameters of the precursors lie between those of $FeC_2O_4·2H_2O$ and $NiC_2O_4·2H_2O$ phasess (Table 7). Therefore, it is speculated that the nickel/iron atoms replaced or substituted for the iron/nickel atoms reciprocally in the process of co-precipitation, with a substitutional solid solution being formed. It means that $NiC_2O_4·2H_2O$ and $FeC_2O_4·2H_2O$ are not formed independently and separately, but homogeneously.

In order to confirm the above hypothesis, a comparative experiment was designed. First, $NiC_2O_4·2H_2O$ and $FeC_2O_4·2H_2O$ were prepared respectively via precipitation method by using $NiCl_2·6H_2O$, $FeCl_2·4H_2O$ and $(NH_4)_2C_2O_4$ as the raw materials under the same conditions. A mechanical mixture was obtained by mixing the prepared $NiC_2O_4·2H_2O$ and $FeC_2O_4·2H_2O$ samples in a planetary ball mill at a speed of 400 r/min for 2 h. TG−DTA curves of different samples are illustrated in Fig. 9. It can

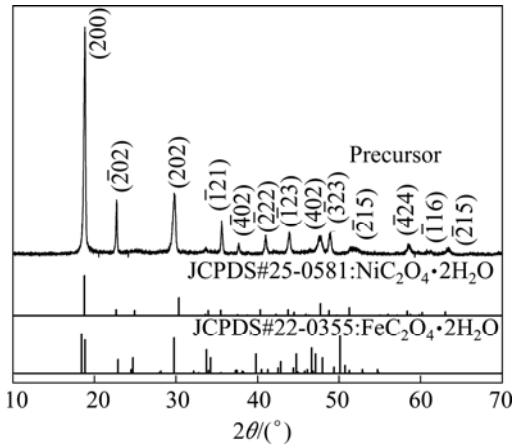

Fig. 8 XRD pattern of precursor

Table 7 Lattice parameters of $FeC_2O_4·2H_2O$, $NiC_2O_4·2H_2O$ and precursors

Sample	*a*/Å	*b*/Å	*c*/Å
Precursor	11.994	5.463	9.818
$FeC_2O_4·2H_2O$	12.05	5.57	9.76
$NiC_2O_4·2H_2O$	11.775	5.333	9.833

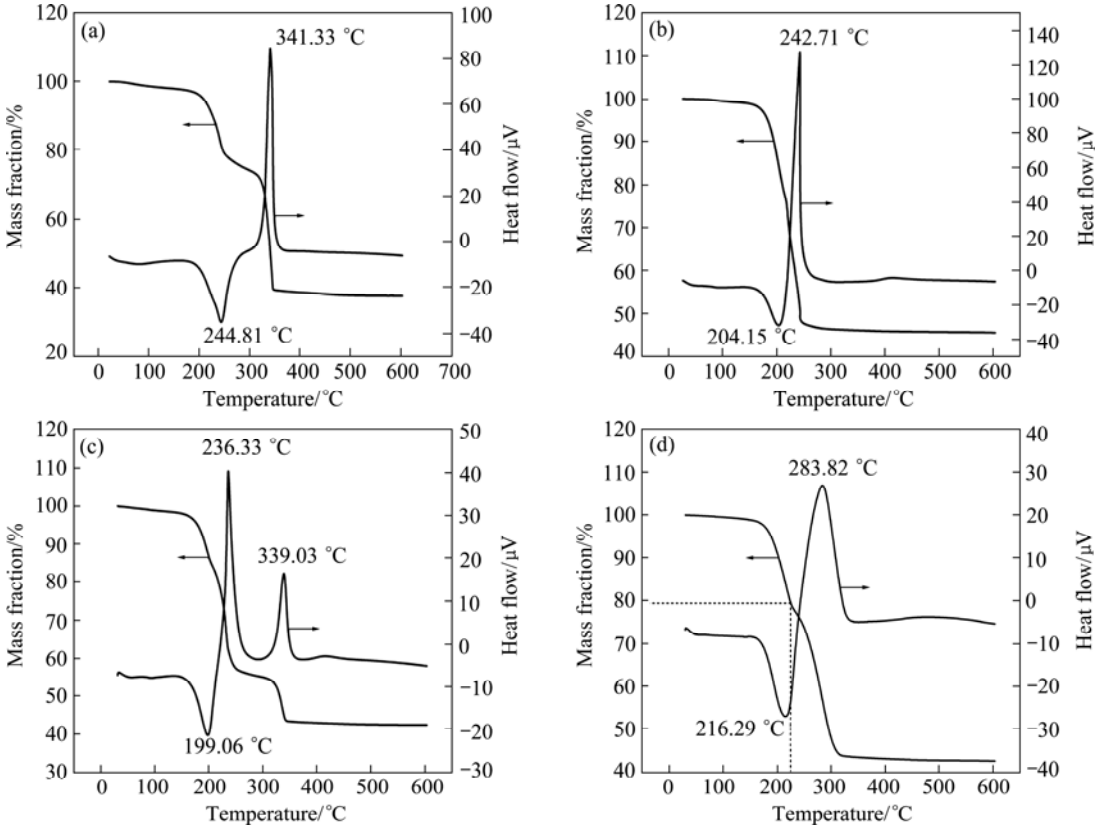

Fig. 9 TG−DTA curves of different samples: (a) $NiC_2O_4·2H_2O$; (b) $FeC_2O_4·2H_2O$; (c) Mixture of $n(NiC_2O_4·2H_2O)$/ $n(FeC_2O_4·2H_2O)$=1/2; (d) Co-precipitate with $n(Ni^{2+})$/ $n(Fe^{2+})$=1/2

obviously be seen that the difference between DTA curves belongs to different samples. For $NiC_2O_4·2H_2O$, $FeC_2O_4·2H_2O$ and co-precipitation precursors, there is only one exothermic peak, and the exothermic peak temperature of co-precipitation precursor (283.82 °C) is between those of $FeC_2O_4·2H_2O$ (242.71 °C) and $NiC_2O_4·2H_2O$ (341.33 °C). But for the mechanical mixed sample, there are two exothermic peaks, corresponding to 236.33 and 339.03 °C, respectively. Comparing with the exothermic peak temperatures of $NiC_2O_4·2H_2O$ and $FeC_2O_4·2H_2O$, it can be observed that the exothermic peaks of the mixture sample are matched with those of $NiC_2O_4·2H_2O$ and $FeC_2O_4·2H_2O$ samples, respectively. Thus, taking all these into consideration, it naturally comes to a conclusion that the precursor obtained from co-precipitation process is solid solution, and it is consistent with the result of XRD analysis. Furthermore, for the as-obtained precursor, the total water mass loss is 20.05% in the temperature range of 30−225 °C (Fig. 9(d)), and it corresponds closely to the theoretical mass loss (19.9%) of mixture of $NiC_2O_4·2H_2O$+ $2(FeC_2O_4·2H_2O)$. Therefore, the chemical formula of the prepared precursors can be simply described as $NiFe_2(C_2O_4)_3·6H_2O$.

Final $NiFe_2O_4$ product is obtained by calcining the precursors at 700 °C for 4 h, and its SEM image and XRD pattern are illustrated in Fig. 10. The results indicate that the prepared $NiFe_2O_4$ product has a single and pure phase, and the size of the product is about 300 nm. The characteristics of $NiFe_2O_4$ product will be reported in the subsequent paper.

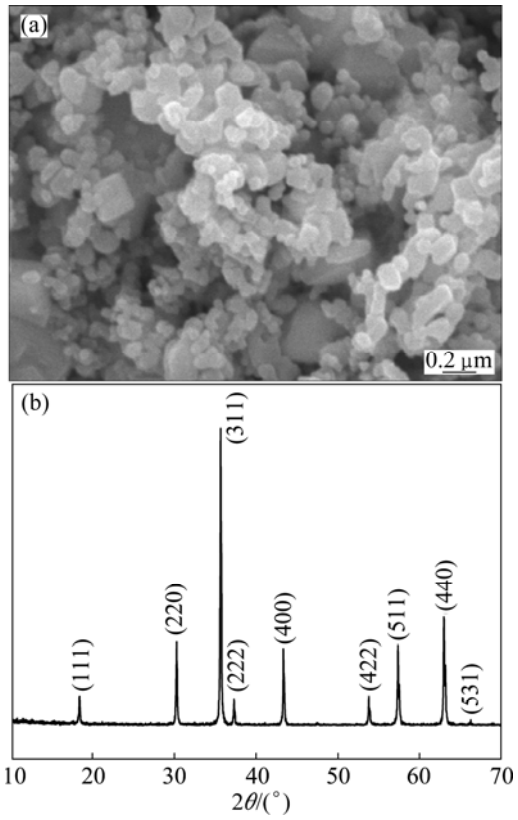

Fig. 10 SEM image (a) and XRD pattern (b) of final $NiFe_2O_4$ product after being calcined at 700 °C for 4 h

5 Conclusions

1) Well-crystallized and fine $NiFe_2(C_2O_4)_3·6H_2O$ precursors for $NiFe_2O_4$ preparation were successfully synthesized via co-precipitation method by using the low-grade nickel matte as raw material.

2) Under the conditions of solution pH=2 and 1.2 times theoretical amount of $(NH_4)_2C_2O_4$ addition, both the precipitation rates of Ni^{2+} and Fe^{2+} are higher than 99.8%. The obtained precursor is substitutional solid solution, wherein the nickel/iron atoms replace or substitute for the iron/nickel atoms reciprocally, indicating that the iron and nickel are mixed on molecular level, which is beneficial for synthesizing stoichiometric $NiFe_2O_4$ in the subsequent heat treating process.

3) Pure and well-crystallized $NiFe_2O_4$ powders are obtained after being calcined at 700 °C for 4 h, and the particle size of the $NiFe_2O_4$ powders is about 300 nm.

References

[1] PILENI M P. Magnetic fluids: Fabrication, magnetic properties, and organization of nanocrystals [J]. Advanced Functional Materials, 2001, 11(5): 323−336.

[2] SUGIMOTO M. The past, present, and future of ferrites [J]. Journal of the American Ceramic Society, 1999, 82(2): 269−280.

[3] SONG Q, ZHANG Z J. Shape control and associated magnetic properties of spinel cobalt ferrite nanocrystals [J]. Journal of the American Chemical Society, 2004, 126(19): 6164−6168.

[4] YANG H M, ZHANG X C, AO W Q, QIU G Z. Formation of $NiFe_2O_4$ nanoparticles by mechanochemical reaction [J]. Materials Research Bulletin, 2004, 39(6): 833−837.

[5] MUROI M, STREET R, McCORMICK P G, AMIGHIAN J. Magnetic properties of ultrafine $MnFe_2O_4$ powders prepared by mechanochemical processing [J]. Physical Review B, 2001, 63(18): 184414−184421.

[6] CEYLAN A, OZCAN S, Ni C, ISMAT S S. Solid state reaction synthesis of $NiFe_2O_4$ nanoparticles [J]. Journal of Magnetism and Magnetic Materials, 2008, 320(6): 857−863.

[7] CEYLAN A, OZCAN S, NI C, ISMAT S S. Investigation of nickel ferrite formation in a binary Fe (III)−Ni (II) hydroxide precipitate containing H_2O with or without Li_2O doping [J]. Journal of Alloys and Compounds, 2009, 486(1−2): 824−829.

[8] DOH S G, KIM E B, LEE B H, OH J H. Characteristics and synthesis of Cu−Ni ferrite nanopowders by coprecipitation method with ultrasound irradiation [J]. Journal of Magnetism and Magnetic Materials, 2004, 272−276: 2238−2240.

[9] CHEN D H, HE X R. Synthesis of nickel ferrite nanoparticles by sol-gel method [J]. Materials Research Bulletin, 2001, 36(7): 1369−1377.

[10] CHATTERJEE A, DAS D, PRADHAN S K, CHAKRAVORTY D. Synthesis of nanocrystalline nickel−zinc ferrite by the sol−gel

method [J]. Journal of Magnetism and Magnetic Materials, 1993, 127(1): 214−218.

[11] GEORGE M, MARY J A, NAIR S S, JOY P A, ANANTHARAMAN M R. Finite size effects on the structural and magnetic properties of sol–gel synthesized $NiFe_2O_4$ powders [J]. Journal of Magnetism and Magnetic Materials, 2006, 302(1): 190−195.

[12] HUO J Z, WEI M Z. Characterization and magnetic properties of nanocrystalline nickel ferrite synthesized by hydrothermal method [J]. Materials Letters, 2009, 63(13): 1183−1184.

[13] ZHOU J, MA J F, SUN C, XIE L J, ZHAO Z Q, TIAN H, WANG Y G, TAO J T, ZHU X Y. Low temperature synthesis of $NiFe_2O_4$ by a hydrothermal method [J]. Journal of the American Ceramic Society, 2005, 88(12): 3535−3537.

[14] FANG J, SHAMA N, TUNG L D, SHIN E Y, O'CONNOR C J, STOKES K L. Ultrafine $NiFe_2O_4$ powder fabricated from reverse microemulsion process [J]. Journal of Applied Physics, 2003, 93(10): 7483−7485.

[15] MISRA R D K, KALE A, SRIVASTAVA R S, SENKOV O N. Synthesis of nanocrystalline nickel and zinc ferrites by microemulsion technique [J]. Materials Science and Technology, 2003, 19(6): 826−830.

[16] AHMED Y M Z, EWAIS E M M, ZAKI Z I. In situ synthesis of high density magnetic ferrite spinel ($MgFe_2O_4$) compacts using a mixture of conventional raw materials and waste iron oxide [J]. Journal of Alloys and Compounds, 2010, 489(1): 269−274.

[17] HESSIEN M M, RASHAD M M, HASSAN M S, EL-BARAWY K. Synthesis and magnetic properties of strontium hexaferrite from celestite ore [J]. Journal of Alloys and Compounds, 2009, 476(1−2) 373−378.

[18] AHMED Y M Z. Synthesis of manganese ferrite from non-standard raw materials using ceramic technique [J]. Ceramics International, 2010, 36(3): 969−977.

[19] RASHAD M M. Synthesis and magnetic properties of manganese ferrite from low grade manganese ore [J]. Materials Science and Engineering B, 2006, 127(2−3): 123−129.

[20] KELLOGG H H. Thermochemistry of nickel-matte converting [J]. Canadian Metallurgical Quarterly, 1987, 26(4): 285−298.

[21] DUCRET A, RANKIN W. Liquidus temperatures and viscosities of $FeO-Fe_2O_3-SiO_2-CaO-MgO$ slags at compositions relevant to nickel matte smelting [J]. Scandinavian Journal of Metallurgy, 2002, 31(1): 59−67.

[22] SPEIGHT J G. Lange's handbook of chemistry, 6th Edition [M]. New York: McGRAW-HILL, 2005.

[23] WANG Jin, LIU Xiao-min, YANG Hui. Synthesis and electrochemical properties of highly dispersed $Li_4Ti_5O_{12}$ nanocrystalline for lithium secondary batteries [J]. Transactions of Nonferrous Metals Society of China, 2012, 22(3): 613−620.

[24] ZOU Min-min, AI Deng-jun, LIU Kai-yu. Template synthesis of MnO_2/CNT nanocomposite and its application in rechargeable lithium batteries [J]. Transactions of Nonferrous Metals Society of China, 2011, 21(9): 2010−2014.

利用低冰镍制备铁酸镍前躯体

何利华[1]，赵中伟[1]，张有新[1,2]

1. 中南大学 冶金与环境学院，长沙 410083；
2. 金川集团股份有限公司，金昌 737104

摘　要：以低冰镍为原料，采用草酸盐共沉淀法合成颗粒细小的铁酸镍前躯体 $NiFe_2(C_2O_4)_3·6H_2O$。$NiCl_2-FeCl_2-(NH_4)_2C_2O_4-H_2O$ 体系的热力学研究表明：Ni^{2+}和 Fe^{2+}的理论最佳共沉淀 pH 值为 2，$C_2O_4^{2-}$ 对 Ni^{2+}、Fe^{2+}离子具有较强的络合作用。在理论研究的基础上，考察沉淀参数对沉淀率和前躯体粒度的影响。结果表明：最佳共沉淀条件为溶液 pH=2，反应温度为 45 ℃，$(NH_4)_2C_2O_4$ 加入量为理论值的 1.2 倍，PEG400 加入量为 3%。在此条件下，Ni^{2+}和 Fe^{2+}的沉淀率达 99.8%，所得前躯体的粒径为 1~2 um。XRD 和 TG−DTA 分析表明：所得前躯体为单相置换固溶体，反应过程中镍、铁原子相互取代。

关键词：铁酸镍；铁氧体；磁性材料；共沉淀；低冰镍

(Edited by Jing-hua FANG)